Dominant factor of zero-field-cooled magnetization in discontinuous Fe films

Yu Shiratsuchi* and Masahiko Yamamoto
Department of Materials Science and Engineering, Graduate School of Engineering, Osaka University, 2-1 Yamadaoka, Suita, Osaka 565-0871, Japan

(Received 20 February 2007; revised manuscript received 26 June 2007; published 29 October 2007)

The zero-field-cooled (ZFC) magnetization under the various field and temperature conditions has been investigated using the discontinuous Fe films. Among the various factors influencing the ZFC magnetization, it is found that either the thermal relaxation or the Langevin behavior dominates the ZFC magnetization, depending on the energy barrier distribution which is altered by the growth temperature. The peak temperature of ZFC magnetization follows the Néel-Brown model for the narrower energy barrier distribution. With broadening the energy barrier distribution for the higher growth temperature, the Langevin behavior of thermally fluctuated particles becomes dominant. The change of energy barrier distribution, namely, the dominant factor of ZFC magnetization, is explained by the broadening of size distribution and the degradation of crystallinity with increasing growth temperature. For both cases, we estimate the superparamagnetic blocking temperature T_B and obtain the effective magnetic anisotropy and the effective volume from the field dependence of T_B. From the obtained values, we show the presence of interparticle interaction for the Fe grown at 323 K, and discuss the effective magnetic anisotropy of randomly oriented particles grown above 573 K.

DOI: 10.1103/PhysRevB.76.144432 PACS number(s): 75.20.−g, 75.75.+a

I. INTRODUCTION

Ferromagnetic nanoparticles are currently the subject of intense research activity partly owing to the development of magnetic storage devices. As a one important topic in the research field on the ferromagnetic nanoparticles, the thermal stability of magnetization has been lively studied.[1–6] Superparamagnetism appears as a result of the thermal fluctuation of magnetization, and from this viewpoint, we have been investigating superparamagnetism of two dimensionally (2D) aligned nanoparticles.[7–9]

Superparamagnetism itself is well known since the pioneering work by Néel in 1949.[10] However, some details remain unclear especially in the interpretation of peak temperature of zero-field-cooled (ZFC) magnetization, even though it is often used to estimate the blocking temperature T_B. When we interpret the peak temperature of ZFC magnetization accurately, one complication is arisen due to the size distribution and/or the energy barrier distribution. The size distribution of nanoparticle is schematically illustrated in Fig. 1. The three different types of magnetic behavior, depending on the particle size, contribute the measured magnetization simultaneously under the size distribution, equivalent to the energy barrier distribution. The dividing volume of the region V_{activate} is determined by the temperature T and the effective magnetic anisotropy strength K_{eff} through the relationship $V_{\mathrm{activate}} \propto k_B T/K_{\mathrm{eff}}$, where k_B is the Boltzmann constant. The magnetization of the smaller (larger) particles, $V \ll (\gg) V_{\mathrm{activate}}$, is magnetically fluctuated (stable) against the thermal agitation, respectively. These types of particles are sometimes described as unblocked (blocked) particles, respectively. The former type of particles obeys the Langevin function and behaves as superparamagnet. In contrast, the latter have the enough large energy barriers against the thermal agitation, and behave as the ordinal ferromagnet having the single magnetic domain. The magnetization of the latter particles rotates around the metastable state below the reversal field. For the particles having the volume $V \approx V_{\mathrm{activate}}$, the magnetization relaxation time τ becomes comparable to the measurement time. Hence, τ has the important role for the magnetization reversal. This means that the thermal activation of magnetization within the measurement time occurs only for the last type of particle having $V \approx V_{\mathrm{activate}}$.

When the blocking temperature is discussed from the peak of ZFC magnetization, the thermal activation of magnetization alone is considered and other contributions from the former two types of particles are not taken into account. However, the significant contributions from the magnetically fluctuated, i.e., $V \ll V_{\mathrm{activate}}$, and the magnetically stable, i.e., $V \gg V_{\mathrm{activate}}$, particles alter the situation dramatically. For instance, the nonlinear magnetization of magnetically fluctuated particles is shown up by the finite field strength, and it sometimes dominates the ZFC magnetization. Thus, in order

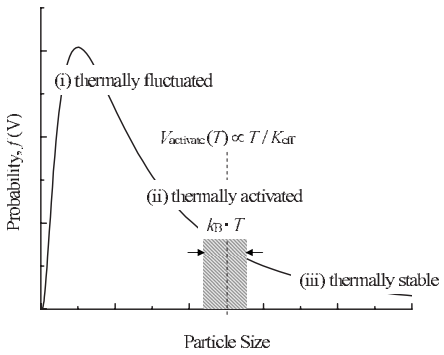

FIG. 1. Schematic representation of size distribution of nanoparticle system. In the presence of size distribution, the thermal activation of magnetization occurs for the particle having the volume $\approx V_{\mathrm{activate}}(T) \propto T/K_{\mathrm{eff}}$. The smaller (larger) particles are magnetically fluctuated (stable) against the thermal agitation, and behave as the superparamagnetic (ferromagnetic) particles, respectively. The actual size distribution is shown in Fig. 3 as a diameter distribution.

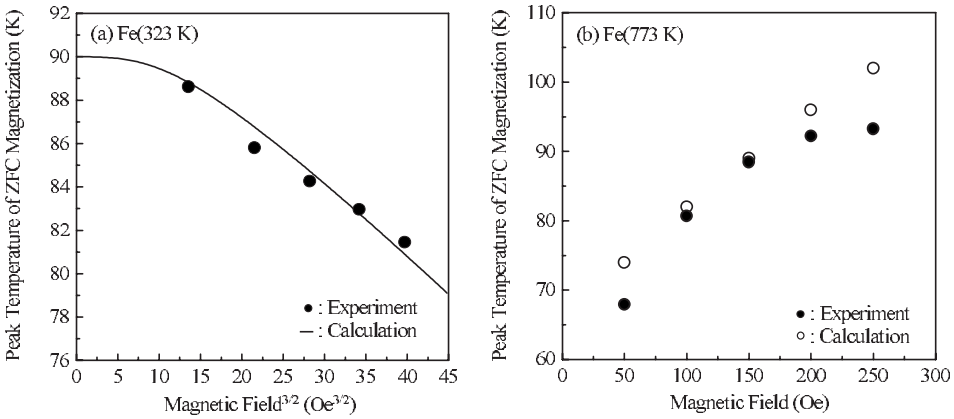

FIG. 2. Magnetic field dependence of peak temperature of ZFC magnetization for Fe particles grown at (a) 323 K and (b) 773 K, respectively. The solid line in (a) represents the calculated results based on the Néel-Brown model. The closed and open circles in (a) and (b) represent the experimentally obtained and calculated values, respectively.

to interpret the physical meanings of the peak of ZFC magnetization precisely, the detailed investigations on the blocking phenomenon under the various field conditions are essential. It might to be noted that even for the monodisperse particle assemblies, the situation is essentially the same as above when the magnetic anisotropy is dispersed.

In our previous report,[7,9] we have shown the characteristic superparamagnetic behavior of 2D distributed Fe nanoparticles. We describe here the important findings in our previous work in order to help understand our motivation in this paper. Changes in peak temperature of ZFC magnetization T_{peak} with the field strength are shown in Fig. 2. T_{peak} behaves in the opposite way for Fe nanoparticle grown at low (323 K) and high (773 K) temperatures, i.e., T_{peak} decreases (increases) with increasing field for the Fe grown at low (high) temperatures, respectively. The former behavior is explained by the thermal activation, namely, the Néel-Brown model. On the contrary, the latter is never explained unless the contributions from the other types of magnetization explained above are taken into account. Thus, it is clear that the dominant contribution to the ZFC magnetization differs for two cases. Considering the different dominant factors of the ZFC magnetization, it is easily expected that its peak temperature would have the different physical meaning. In this paper, we examine the magnetic response of superparamagnetic particles under the various field and temperature conditions in detail. From these investigations, we provide the interpretation of T_{peak} and clarify the dominant factor of T_{peak} for the above two cases. We discuss the estimation of actual blocking temperature, its field dependence, and the existence of interparticle interactions, as well.

II. EXPERIMENT

Fe particles were fabricated via the Volmer-Weber growth of ultrathin film. In this fabrication method, the particles distribute two dimensionally on the substrate. It is speculated that the 2D aligned particles could reduce the magnetic anisotropy dispersion compared to the three dimensional particles such as the granular films especially for the epitaxially grown particles. Ultrathin (1.0 nm thick) Fe films were prepared by VG-80M molecular beam epitaxy system. The base pressures before and during growth were typically below 4×10^{-9} and 5×10^{-8} Pa, respectively. The growth rate of Fe was 0.005 nm/s. The growth temperature was varied in the range of 323–773 K. Hereafter, we describe the Fe grown at T_s as Fe(T_s), for example, Fe grown at 323 K as Fe (323 K). To investigate the magnetic properties, the Fe films have to be exposed to air. In order to avoid the surface oxidization, 10-nm-thick Au capping layer was deposited at room temperature. We confirmed the lack of oxidation indirectly from the fact that the magnetization curves at 10 K show no shift after cooling in field (10 kOe). We used α-Al_2O_3(0001) surface as a substrate in order to promote the Volmer-Weber growth of Fe. The substrate was annealed in air at 1273 K to flatten the surface before introducing the vacuum system. After that, it was cleaned in UHV chamber by annealing for several hours at 1173 K just before Fe deposition.

The magnetic properties were investigated by means of the superconducting quantum interference device magnetometry. Our investigation encompassed the temperature dependence of field-cooled (FC), ZFC, and remanent (RM) magnetization in the temperature range of 5–300 K under the in-plane magnetic fields from 10 to 250 Oe. The measurements were performed during the heating process. Especially, two types of RM are measured after FC and ZFC, called as the thermoremanent magnetization (TRM) and the isothermal remanent magnetization (IRM), respectively.[1,11] For instance, when TRM was measured, the sample was cooled from the enough high temperature, room temperature to the measurement temperature under the certain field. After reaching measurement temperature, the field was removed and the magnetization was measured. In the case of IRM, the similar procedure was done after ZFC procedure. TRM and IRM give the magnetization from the magnetically stable particles and the magnetically activated particles at the measurement temperature, respectively.

The structure of Fe film was investigated using the atomic force microscopy operated with a noncontact mode (NC-AFM). The investigation of surface structure was performed *in situ* before Au coating. The crystallographic orientation perpendicular to the film was examined by means of the x-ray diffraction (XRD) method. XRD measurement was performed with Cu $K\alpha$ irradiation. For XRD measurement, 1.0-nm-thick Fe film is too thin, and the sensitivity of XRD is not enough for the detection of diffraction peaks. In this study, XRD measurement was performed using 2.0-nm-thick Fe film from which the crystallographic orientation of

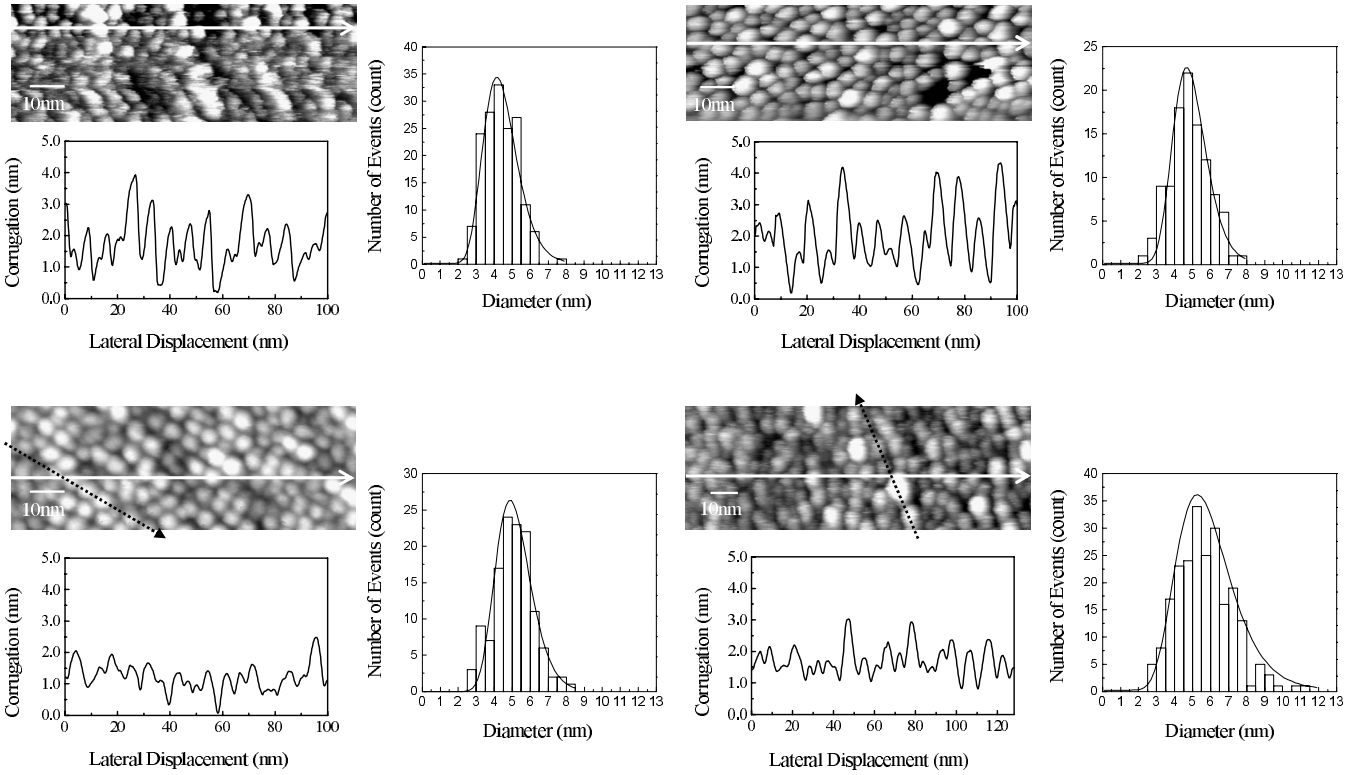

FIG. 3. Surface structure and diameter distribution of Fe particle arrays grown at (a) 323 K, (b) 473 K, (c) 573 K, and (d) 773 K, respectively (Ref. 7). The cross sectional view corresponding to the solid arrow in AFM images is shown below AFM images. The diameter distribution is estimated from the several AFM images. The dotted arrows in (c) and (d) show the particle alignment direction.

1.0-nm-thick Fe was expected indirectly. Note that 2.0-nm-thick Fe film is not the perfect continuous film, and the discontinuous part is still remaining.[12]

III. RESULTS AND DISCUSSIONS

A. Structure of the discontinuous Fe films

The surface structure and the diameter distribution of Fe particles are shown in Fig. 3.[7] The particles are observed for all investigated Fe films, and the diameter distribution is expressed by the log-normal distribution, as expected in Fig. 1. The mean particle volume and the standard deviation assuming the spherical shape are shown in Table I. While the particle distribution is overlapped for the Fe grown at different temperatures due to the wide distribution, the particle size tends to increase with increasing growth temperature. The details of the obtained structural parameters are discussed together with the correlation to the magnetism in the Sec. III D. Besides the particle size, the shape and the alignment also change with the growth temperature. For the growth temperature $\leqslant$473 K [Figs. 3(a) and 3(b)], the diameter and

TABLE I. Magnetic parameters obtained from the field dependence of blocking temperature. Some structural parameters estimated from AFM observation are also presented.

		T_s (K)			
Estimation		323	473	573	773
T_B vs H	T_{B0} (K)	46±2	21±2	24±1	31±2
	K_{eff} (10^5 erg cc^{-1})	0.59±0.1	12.0±0.8	10.1±0.4	10.0±0.4
	V_{mag} (nm^3)	1190±40	72±4	97±4	125±6
	ξ (dimensionless)	$(1.6\pm0.1)\times10^{-4}$	Noninteracting	Noninteracting	Noninteracting
$f(T_B)$ vs T	σ_{T_B} at 50 Oe (K)	12.1	13.3	16.8	14.2
AFM	V_{AFM} (nm^3)[a]	25 (D=3.6 nm)	33 (D=4.0 nm)	39 (D=4.2 nm)	59 (D=48 nm)
	σ_D (nm)	0.94	1.06	1.07	1.54

[a]V_{AFM} is estimated using the diameter estimated from AFM observation under the assumption of the spherical shape.

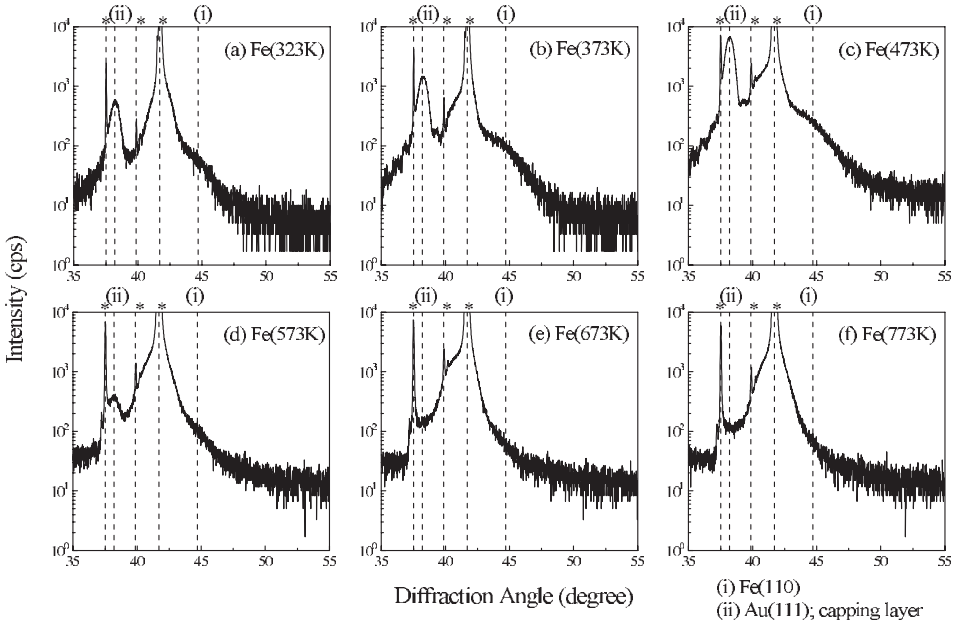

FIG. 4. XRD profiles of 2.0-nm-thick Fe films. The symbol " * " represents the diffraction peak from α-Al_2O_3 substrate; α-Al_2O_3(0006) by Cu $K\alpha$, Cu $K\beta$ W $L\alpha_1$ from the strong peak.

the height are almost the same, namely, the particles are nearly spherical. Concerning the particle alignment, any special alignment is not observed, although the thermal drift is observed in Fig. 3(a). Increasing the growth temperature above 573 K, the diameter becomes larger than the height [Figs. 3(c) and 3(d), cross sectional view]. In other words, the particle shape deviates from the sphere and changes into the disk. In addition to the change of shape, it is observed that Fe particles align one dimensionally as indicated by the dotted arrow. The alignment direction is not coincident to the step direction of substrate. As mentioned later, the crystalline quality of Fe degrades at the high growth temperature probably due to the large difference of thermal expansion rate of Fe and α-Al_2O_3 substrate. Considering the change of particle alignment together with the degradation of crystalline quality, it is possible that the interface strain between Fe and the substrate would influence on the particle alignment by generating the elastic interaction between Fe particles. However, at the present stage, any experimental results to support the discussion are not obtained, and thus the reason for the regular particle alignment is not clear.

In addition to the particle size, the crystallinity also depends on the growth temperature. XRD profiles of 2.0-nm-thick Fe films are shown in Fig. 4. For Fe grown below 473 K, the diffraction peaks from Fe(110) and the capped Au(111) are clearly observed although the peak from Fe(110) is quite broad due to the low thickness of 2.0 nm. Both peaks are weakened above the growth temperature of 573 K, and vanish for Fe grown above 673 K. Above 673 K, any diffraction peaks except for α-Al_2O_3 substrate are not observed. This means that the Fe grows with bcc(110) plane below 473 K, and becomes polycrystalline above 673 K. Considering that the peak from Fe(110) almost vanishes at the intermediate growth temperature of 573 K, the crystallographic orientation of Fe starts to degrade at 573 K. The influence of degraded crystallinity on the magnetic properties is discussed in Sec. III D.

B. Interpretation of T_{peak} and estimation of T_B

As shown in Fig. 2(a), T_{peak} of Fe (323 K) decreases with increasing field. This feature is observed for Fe grown below 473 K. The field dependence of T_{peak} is reproduced by the phenomenological calculation based on the Néel-Brown model [the solid line in Fig. 2(a)], i.e., $T_{peak} \propto H^2 (H \ll H_K)$, $T_{peak} \propto H^{2/3} (H < H_K)$.[13–15] Note that the high-field $H^{2/3}$ dependence cannot be seen from the Néel-Brown formula in the mathematical form, but the calculations based on Brown's formula have shown this power law dependence for the high field, $H < H_K$. The detail of calculation method is described later. The correspondence between the experiment and the calculation means that the thermal activation of magnetization actually occurred around T_{peak}. Thus, it looks that T_{peak} represents the superparamagnetic blocking temperature. However, since T_{peak} and ZFC magnetization are measured under the finite field, the contribution from the magnetically reversible particles, i.e., Langevin behavior of magnetically fluctuated and the reversible magnetization rotation of the magnetically stable particles, is also involved in the measurement. In this case, there is a possibility to overestimate the blocking temperature. In fact, the actual superparamagnetic blocking temperature is smaller than T_{peak}, as shown later.

The extent of contribution from each type of particles depends on the width of the size distribution, more precisely the energy barrier distribution. Hence, there should be the case that either the thermally equilibrated behavior (Langevin behavior) of magnetically fluctuated particles or the reversible magnetization rotation of magnetically stable particles dominates the ZFC magnetization. In this case, T_{peak} does not follow the Néel-Brown behavior, but shows the other type of field dependence. In fact, as shown in Fig. 2(b), for Fe particles grown at high temperature of 773 K, T_{peak} increases with increasing magnetic field strength, which is never explained by the Néel-Brown model. The increase of T_{peak} has been observed in other systems,[16,17] and it is some-

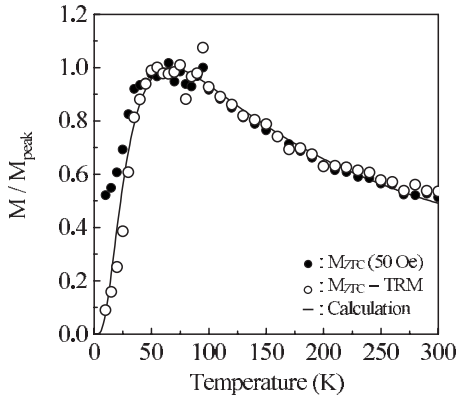

FIG. 5. Temperature dependence of magnetization for Fe grown at 773 K. The closed and open circles represent the ZFC magnetization and the difference between ZFC magnetization and TRM, respectively. The solid line represents the calculated results based on the Langevin function.

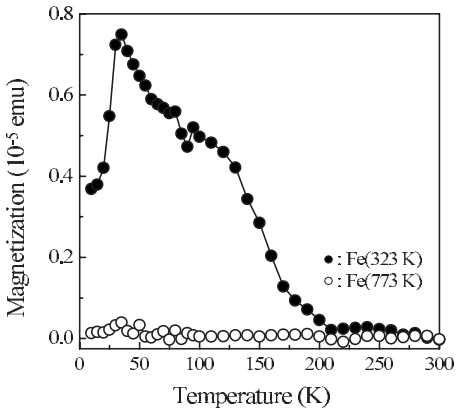

FIG. 6. Temperature dependence of IRM. The closed and open circles represent the values for Fe grown at (a) 323 K and (b) 773 K, respectively.

times interpreted by the increase of energy barrier for magnetization rotation. However, in our case, the actual blocking temperature, namely, the energy barrier for magnetization reversal decreases with increasing field, as shown later. In order to explain the increase of T_{peak}, Hanson *et al.* considered the observed behavior of T_{peak} from the viewpoint of the different contributions to the ZFC magnetization.[17] Following their treatment, we have calculated the ZFC magnetization by using the formulas,

$$M_{\text{ZFC}} = \int_0^{V_{\text{activate}}(T)} M(x),$$

$$V_{\text{activate}}(T) = \frac{25k_BT}{K_{\text{eff}}},$$

$$M(x) = M_S \frac{\pi}{6} x^3 f(x) dx L(a),$$

$$L(a) = \coth(a) - \frac{1}{a},$$

$$a = M_S \frac{\pi}{6} x^3 H/k_BT \qquad (1)$$

where K_{eff} is the effective magnetic anisotropy energy (here, we assume the bulk magnetocrystalline anisotropy, 4.7×10^4 J/m^3 for simplicity), M_S is the saturation magnetization (2.1 T), x is the particle diameter, $f(x)$ is the probability function of particle diameter, $L(a)$ is the Langevin function, k_B is the Boltzmann constant, and T is the absolute temperature. Equation (1) gives the contribution from the magnetically fluctuated particles alone. The results are shown in Fig. 5. In the figure, the experimentally obtained ZFC magnetization of Fe (773 K) is also shown by the closed circles. It is clear that Langevin behavior, i.e., the contribution from magnetically fluctuated particle, alone generates the peak in ZFC magnetization. The experimental results (closed circle) are well represented by the calculation (solid line) in the temperature region above T_{peak}. In Fig. 5, it is seen that the calculated results deviate from the experimental values in the low temperature regime. This deviation is due to the contribution from the magnetically stable particles due to the small thermal energy which is obtained by TRM. The subtracted signal from ZFC magnetization, $M_{\text{ZFC}}-\text{TRM}$ (open circle in Fig. 5), is well fitted to the calculated result for the whole temperature range. The clear correspondence between the calculated results and $M_{\text{ZFC}}-\text{TRM}$ strongly supports the discussion that T_{peak} is dominated by the magnetically fluctuated particle. Besides the temperature dependence of the ZFC magnetization, the calculated T_{peak} increases with the field strength and also corresponds to the experimental results qualitatively [Fig. 2(b), open circles]. The agreement of the experiment with the calculation based on Langevin function means that the thermal activation of magnetization does not affect the measured magnetization crucially around T_{peak}, and thus T_{peak} does not represent the superparamagnetic blocking temperature. It is worth to note that the peak in the calculated ZFC magnetization is not generated by the only linear term of Langevin function but by the combined result of the nonlinear term of Langevin function and the size distribution.

Here, we summarize the above results on the field dependence of T_{peak} and its dominant contribution briefly to help understand the following verification. For the Fe grown at the low temperature ($\leqslant$473 K), the thermal activation has the dominant contribution around T_{peak}, and thus T_{peak} follow the Néel-Brown model. On the other hand, for the Fe grown at the high temperature ($\geqslant$573 K), Langevin behavior of magnetically fluctuated particles well expresses the other types of experimental results on the temperature dependence of ZFC magnetization and the field dependence of T_{peak}. Since these two factors have the quite different relaxation time, the remarkable difference appears in the remanent state. Thus, it is possible to verify the change of dominant factor from the temperature dependence of IRM, which is shown in Fig. 6. For the case that the thermal activation has the dominant role, IRM is observable in the almost whole temperature range (closed circles), and it has the peak around

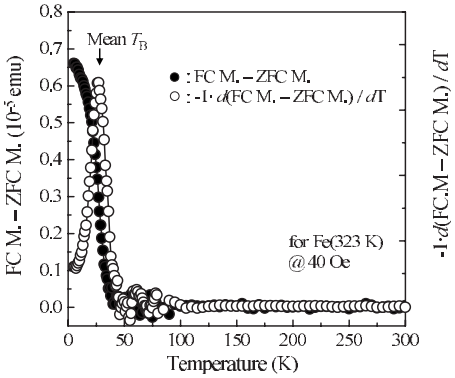

FIG. 7. Estimation of superparamagnetic blocking temperature. The closed circles represent the difference between FC and ZFC magnetizations (left axis). The open circles represent the temperature dependence of closed circles (right axis), and its peak temperature is the mean superparamagnetic blocking temperature. In the figure, the result of Fe (323 K) under the magnetic field of 40 Oe is presented as an example.

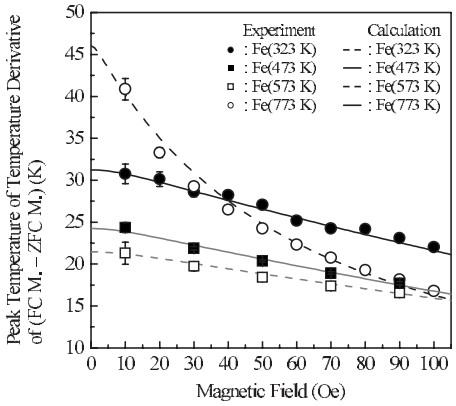

FIG. 8. Magnetic field dependence of blocking temperature. The symbols represent the experimental values and the lines represent the calculated results based on the Néel-Brown model. (see text). The results are presented for Fe (323 K) (open circle, black dotted line), Fe (473 K) (open square, gray dotted line), Fe (573 K) (closed square, gray solid line), and Fe (773 K) (closed square, black solid line), respectively.

the peak in ZFC magnetization. The nonzero IRM is the signature that the irreversible magnetization reversal occurs during the measurement. Possible mechanisms of irreversible magnetization are the thermal activation of magnetization within the individual particles and/or the magnetic correlation due to the interparticle interaction. Although the latter case could occur as mentioned in the next section, even in this case, the superparamagnetic blocking within the individual particles has to be involved. Thus, the above result clearly shows that the thermal activation actually has the significant influence on the ZFC magnetization and T_{peak}. Contrary to the first case, when Langevin behavior expresses the ZFC magnetization, IRM should be vanished. As shown by the open circles, IRM is zero within the experimental error for the whole temperature regime except for the small value around 40 K. The observed features of IRM exactly agree with the above conclusion that the Langevin behavior of magnetically fluctuated particles dominates the ZFC magnetization.

We have investigated the actual superparamagnetic blocking temperature T_B. T_B is often estimated by the peak temperature of ZFC magnetization T_{peak}. However, as described above, it is not always true that the thermal activation occurs around T_{peak} most frequently within the measurement time. For this problem, we analyze the temperature dependence of magnetization, and estimated T_B from the ZFC magnetization and the FC magnetization by the following method.[11,18] Considering that T_B also distributes in the presence of size distribution, and the distribution of T_B, $f(T_B)$ is obtained by the following formula:

$$f(T_B) \propto -\frac{d(M_{\text{FC}} - M_{\text{ZFC}})}{dT}. \tag{2}$$

The experimentally obtained $f(T_B)$ by using Eq. (2) is shown in Fig. 7. In the figure, the results for Fe (323 K) under the magnetic field of 40 Oe is shown as a typical example. We estimate the mean blocking temperature from the peak of $f(T_B)$. Considering the relationship between the M_{FC}, M_{ZFC}, TRM, and IRM,[1,11]

$$M_{\text{FC}} - \text{TRM} = M_{\text{ZFC}} - \text{IRM}. \tag{3}$$

The same treatment might be possible from TRM and IRM, in principle. However, one should keep in mind that relationship (3) is valid for the ideal superparamagnet, and is not under some deviation from the ideal case, for example, under the interparticle interactions[1] or under the relatively high magnetic field even below the anisotropy field.

The field dependence of the mean blocking temperature estimated by the above treatment is shown in Fig. 8. The error bar is originated from the fitting error, not the measurement error. The mean blocking temperature decreases with increasing magnetic field for all investigated Fe, namely, independent of the dominant factor of the ZFC magnetization. Furthermore, the experimentally obtained T_B values are well represented by the calculation based on the Néel-Brown model (solid and dotted lines). We note that the results for Fe (323 K) are never reproduced unless the interparticle interactions are included. The interparticle interactions for Fe (323 K) are discussed in Sec. III C. Here, we describe the calculation method[14] based on Néel-Brown model briefly. In this model, the relaxation time of magnetization τ is given by

$$\tau^{-1} = \frac{1}{2} f_0 (1 - h_{\text{eff}}^2)\{(1 + h_{\text{eff}})\exp[-a_{\text{eff}}(1 + h_{\text{eff}})^2]$$

$$+ (1 - h_{\text{eff}})\exp[-a_{\text{eff}}(1 - h_{\text{eff}})^2]\},$$

$$f_0 = \sqrt{a_{\text{eff}}}\gamma_0 H_K/\sqrt{\pi},$$

$$h_{\text{eff}} = H/H_K,$$

$$a_{\text{eff}} = \Delta E/k_B T,$$

$$H_K = 0.96 K_{\text{eff}}/M_S,$$

$$\Delta E = K_{\text{eff}} \cdot V_{\text{mag}} + \xi M s^4 V_{\text{mag}}^2 / 3 k_B T, \quad (4)$$

where f_0 is the Larmor frequency, γ_0 is the gyromagnetic factor, H_K is the anisotropy field, ΔE is the energy barrier for the magnetization reversal, k_B is the Boltzmann constant, T is the absolute temperature, and ξ is the interparticle interaction strength assuming the dipole interactions, respectively. In the calculation, we define the blocking temperature as the temperature at which τ becomes equal to the measurement time, 100 s. From the fitting procedures, some magnetic parameters are obtained and are listed in Table I. It is worth to mention that not only T_B at zero fields T_{B0} but also the effective magnetic anisotropy K_{eff} and the magnetic effective volume V_{mag} are separately obtained from the fitting. The separated estimation of K_{eff} and V_{mag} gives further insights of the thermal stability of Fe under the finite field strength. Fe (323 K) shows the high T_{B0} value, but T_B decrease faster than the other Fe due to the large V_{mag}. In contrast, while T_{B0} of Fe (773 K) is lower than that of Fe (323 K), the decrease of T_B is highly suppressed owing to the large K_{eff} and the small V_{mag}. Finally, T_B's of Fe (323 K) and Fe (773 K) are reversed and Fe (773 K) become more stable above the magnetic field of 40 Oe. This is understood by considering Zeeman energy under the finite field. Zeeman energy is proportional to V_{mag}, but is independent on K_{eff}. Since the decrease of energy barrier under the finite field is due to Zeeman energy, the energy barrier under the finite field decreases faster for the larger particle even when T_{B0} is similar.

Another focusing point in the obtained parameter is the difference between V_{mag} and V_{AFM}. Since V_{mag} is estimated from the magnetic measurements, it represents the magnetically effective volume. On the contrary, V_{AFM} is the physical volume of Fe particles estimated from NC-AFM observation. As listed in Table I, for Fe (323 K), V_{mag} is highly larger than V_{AFM}. This fact indicates the enlargement of the magnetically effective volume due to the interparticle interaction.[18,19] The presence of interparticle interaction is investigated in Sec. III C. V_{mag} and V_{AFM} for Fe grown at higher temperature are also different. It is probably due to the difference in the fixed parameters in the above calculation such as the measurement time τ (in this study, fixed at 100 s), the expression of anisotropy field H_K.

C. Interparticle interactions between Fe particles

Considering the dipole interaction, the dipole fields could become larger with decreasing particle distance and increasing particle size. In this study, since the magnetic particles were fabricated by the Volmer-Weber growth of ultrathin film keeping the nominal thickness (total volume), the smaller particles result in the closer distance between the neighboring particles. Thus, the dipole interactions could become larger with decreasing Fe particle size. Of course, the smaller particles give rise to the small magnetization value and results in the decrease of dipole field. However, since the dipole interaction energy is proportional to M_S^2 and r^{-3}, the increment owing to the close distance is faster than the decrease due to the small M_S. Consequently, the decreasing size and the closing distance would generate the larger dipole interaction.

In this section, we investigate the interparticle interactions in Fe (323 K) presenting some signature of interparticle interactions, i.e., the large V_{mag}, the small K_{eff}, and the nonzero ξ. The temperature dependent interparticle interactions result in the peak in temperature dependence of magnetization after cooling under the magnetic field, i.e., FC procedure, as well. The temperature dependence of magnetization is shown in Fig. 9. The Fe (323 K) present the peak in both the FC and ZFC magnetizations, whereas the Fe (773 K) show the peak only in the ZFC magnetization. The peak in FC magnetization is sometimes explained by the phase transition due to the interparticle interactions, for example, the superspin glass state.[20–24]

Here, we investigate the magnetic state at low temperature using the thermal equilibrium magnetization M_{eq}. As well known, for the noninteracting superparamagnet, the peak in the temperature dependence of ZFC magnetization and the difference of FC and ZFC magnetizations are observed. However, this is a valid knowledge within the realistic measurement time since these characteristics of superparamagnet are the results from the change of relaxation time with temperature, not the phase transition. This means that if the system falls into the thermal equilibrium state after the infinite waiting time, above characteristics disappear. After reaching the equilibrium state, the temperature dependence of magnetization would obey the Curie-Weiss law independent of the cooling condition. On the other hand, for the interacting system, M_{eq} might differ from the Curie-Weiss behavior at least although the thermal equilibrium state of the interacting system is not definite. However, it is unrealistic to wait for the extremely long time to access the thermal equilibrium state. In this study, we adopt the method which Mamiya *et al.* demonstrated.[21] They have shown that the system is possible to fall into the thermal equilibrium state by cooling down, maintaining the ratio of magnetic field H and temperature T, called as HT cooling. The estimated M_{eq} value is shown in Fig. 9 by the closed triangle. The Curie-Weiss law is also shown in Fig. 9(b) by the solid line. It is clearly seen that M_{eq} does not obey the Curie-Weiss law for Fe (323 K), while it almost does for Fe (773 K). In order to clarify the detailed magnetic state of Fe grown at 323 K, the characteristic effects of superspin glass state, i.e., the aging effect[22–24] and the memory effect,[20,23,24] have been investigated, but neither effect is observed (not shown). Instead, the other type of memory effect is observed in our Fe particles. The measured result on the memory effect of Fe (323 K) is shown in Fig. 10. The memory effect was measured after stopping the cooling temporally at 30 K for 10^4 s. The measurements were performed during the heating process after zero-field cooling, and thus the observed feature is not affected by the magnetic field but by the interparticle interactions.[24] In the superspin glass system, the memory effect is observed as the reduction of magnetization with respect to the reference value due to the frustration of magnetization.[20,23,24] Whereas in our case, the magnetization after the temporal stop becomes larger than the reference value without stopping of zero-field cooling, as clearly seen in Fig. 10. Furthermore, the magnetization after the temporal stop is constant until reaching temperature at which it be-

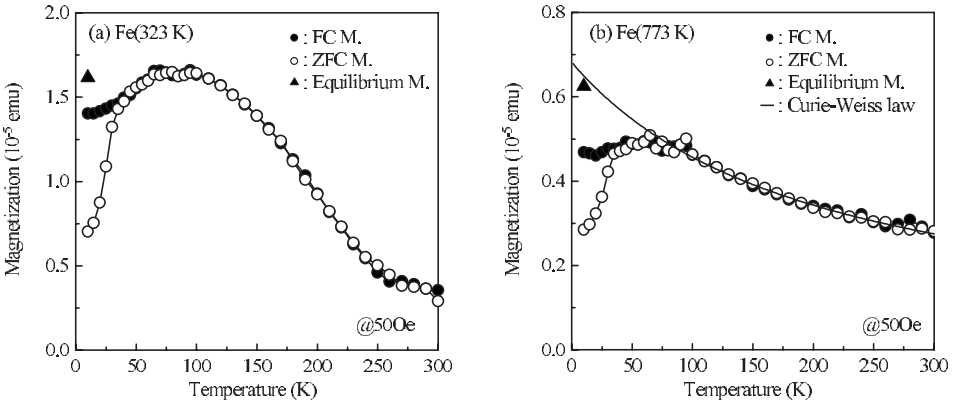

FIG. 9. Temperature dependence of magnetization for Fe grown at (a) 323 K and (b) 773 K. The closed and open circles show FC and ZFC magnetizations, respectively. The closed triangle represents the thermally equilibrium magnetization M_{eq} obtained by *HT* cooling procedure. The detailed method of *HT* cooling should be referred in the text and Ref. 21. The solid line in (b) shows the Curie-Weiss law.

comes the same as the reference value. The magnetization value after reaching constant and the vanishing temperature of memory effect are dependent on the temporally stopped temperature. The observed anomalous memory effect, namely, the positive memory effect, is probably due to the formation of the magnetically collected clusters, whose size is dependent on the temperature, by the ferromagnetically driving interactions. The detailed interpretation on the observed anomalous memory effect is outside the scope of this paper, and thus we will report the details elsewhere. Considering some above mentioned features such as the large V_{mag}, the small K_{eff}, the nonzero value of ξ, the deviation from the Curie-Weiss law of M_{eq}, and the anomalous memory effect, we believe that several Fe particles are magnetically collected due to the interparticle interactions.

D. Structural correlation with magnetic properties

As shown in Fig. 3 and Table I, the mean particle size and the standard deviation of size distribution tend to increase with increasing growth temperature. The observed broadening of size distribution, namely, the size uniformity, correlates to the change of dominant factor of ZFC magnetization. The correlation between the structure and the magnetic properties is summarized in Fig. 11. Both changes in surface structure and dominant factor of ZFC magnetization occur between 473 and 573 K. As also shown in Table I by σ_D, the size distribution is broadened with increasing growth temperature. For the low growth temperature, the thermal relaxation is easy to observe owing to the narrower size distribution. When the size distribution becomes broader, the thermal relaxation is screened by the other contributions from the magnetically fluctuated and stable particles. Especially, it is likely that the contribution from the magnetically fluctuated particles is stronger than that of magnetically stable particles due to the log-normal distribution of particle size. The situation is easy to understand coming back to the schematic representation shown in Fig. 1 and the actual size distribution in Fig. 3.

In addition to the size uniformity, the crystallinity influences the magnetic properties through the anisotropy dispersion, as well. As mentioned in Sec. III A and shown in Fig. 4, the crystallinity depends on the growth temperature. Below the growth temperature of 473 K, the crystallographic orientation of Fe particles would be aligned. In contrast, above the growth temperature of 573 K, Fe particles have the random crystallographic orientation. The change of crystallinity occurred between 473 and 673 K is also coincident with the change of dominant factor of ZFC magnetization discussed in the Sec. III B. The degradation of crystallinity results in the magnetic anisotropy dispersion through the crystallographic orientation dispersion, and resultantly, the magnetic reversal energy barrier distribution is also broadened. Since the broadening of energy barrier distribution gives essentially the same situation of broad size distribution, as described in Sec. I, the crystallographic degradation promotes the broadening of energy barrier distribution in addition to the structural size broadening shown in Fig. 3 and Table I. The broadened energy barrier distribution gives rise to the significant contribution of Langevin behavior of thermally fluctuated particle as discussed above.

Here, we discuss the nonzero K_{eff} value, shown in Table I, of polycrystalline Fe grown above 673 K. As shown in Fig. 4, the diffraction peak from Fe vanishes above the growth

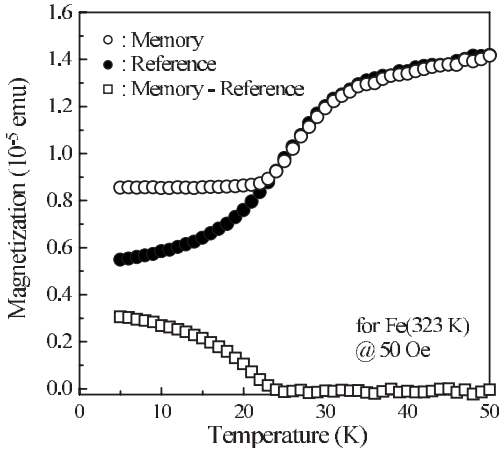

FIG. 10. The memory effect of Fe particle grown at 323 K. The open and closed circles represent the memory and the reference curve, respectively, and the open square represents the difference of the memory and the reference. The memory and reference measurements have been made after zero-field cooling. The memory effect has been measured after the temporal stop of cooling at 30 K for 10^4 s.

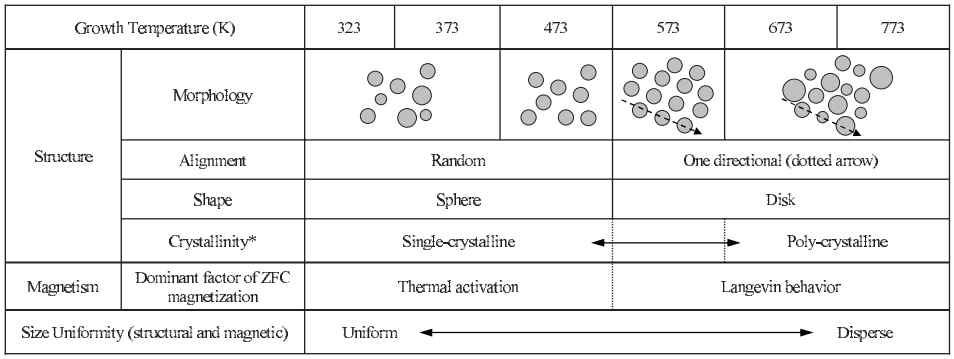

FIG. 11. Correlation of magnetic properties and structure. The change of dominant factor of ZFC magnetization occurs between 473 and 573 K. This temperature range is well coincident with that of the surface structural change.

temperature of 573 K, and thus Fe film should be polycrystalline. However, it is considered that the 2.0-nm-thick Fe films are constructed of the percolation of isolated particles which are already formed at the lower thickness by the Volmer-Weber growth. Based on this consideration, we propose the following percolation mechanism. Before percolation, the individual Fe particle formed in 1.0-nm-thick film would be single crystalline but the crystallographic orientation of Fe particles is random. In the percolation process, the randomly oriented particles contact physically, and resultantly, the grain boundary is created. Even in this model, when the randomly oriented Fe particle percolates into the continuous film, the film becomes polycrystalline. In the percolation process, the effective magnetic anisotropy energy would decrease due to the exchange coupling of the randomly oriented particles, namely, the anisotropy dispersion. After completing the percolation, the magnetic properties are described by assuming the zero K_{eff} as the continuous polycrystalline film. According to the proposed percolation mechanism, the single-crystalline individual Fe particle before percolation has the nonzero magnetocrystalline anisotropy due to the single-crystalline nature. Additionally, the disk shape of Fe particle shown in Fig. 3 and the interface anisotropy at the interfaces of Fe/α-Al_2O_3 and Fe/capped Au might have some contribution to K_{eff} as the shape anisotropy and the interface anisotropy, respectively. The above discussion is supported by the magnetic state of the partly continuous 2.0-nm-thick Fe films, which has been reported previously.[12] In the partly continuous 2.0-nm-thick Fe film, the superparamagnetic state is residual for the polycrystalline Fe film grown at 773 K. Instead, the 2.0-nm-thick Fe film grown at 473 K having the similar film structure shows the ferromagnetic behavior at room temperature.

Change of crystallinity would have some role on the change of dipole interaction, as well. Assuming the dipole interaction, the direction of magnetic easy axis determines the dipole field direction. Since the magnetic easy axis of magnetocrystalline anisotropy is determined by the crystallographic orientation and its in-plane alignment, the epitaxial relationship between Fe and α-$Al_2O_3(0001)$ substrate would have some influence on the dipole interactions. Considering the change of epitaxial growth of Fe, the magnetic easy axis of particles is aligned at low growth temperature, but it distributes at the high growth temperature. The dispersion of magnetic easy axis results in the dispersion of dipole field, and thus the dipole interactions should not strongly affect the magnetic properties in the high growth temperature region.

IV. SUMMARY

The ZFC magnetization under the various field and temperature conditions has been investigated for the discontinuous Fe films grown at the various temperatures. Especially, which type of particles in the size distribution, namely, the magnetically fluctuated (unblocked), the thermally activated, or the magnetically stable (blocked) particles, has the dominant contribution is examined. For the growth temperature below 473 K, the field dependence of T_{peak} follows the Néel-Brown model, and IRM has the peak around T_{peak}. These are the clear features showing that the thermal activation has the dominant role in the ZFC magnetization owing to the narrow energy barrier distribution. Especially for Fe grown at 323 K, some signatures of interparticle interactions are also obtained. Increasing growth temperature gives rise to broaden the size distribution, and resultantly, the contribution of magnetically fluctuated particles becomes significant. Above the growth temperature of 573 K, T_{peak} shows the opposite field dependence to the Néel model. This strange behavior is explained by the combined effect of the nonlinear term of Langevin function due to the finite field strength and the size distribution. Furthermore, from the facts that the zero IRM in almost whole temperature range and the coincidence between the experimental results and the model calculation based on the Langevin behavior, it is concluded that the Langevin behavior of magnetically fluctuated particles dominates the ZFC magnetization.

We also provide the actual superparamagnetic blocking temperature. The blocking temperature decreases with increasing field strength independent of the dominant factor of ZFC magnetization. From the investigation on the field dependence of the blocking temperature, several magnetic parameters are obtained. Our treatment gives the energy barrier of magnetization reversal under the zero fields, the effective magnetic anisotropy energy, and the magnetically effective volume separately.

The observed change of dominant factor is discussed from the viewpoint of the energy barrier distribution. The energy barrier is broadened not only by the size distribution but also by the magnetic anisotropy dispersion which is related to the

crystallinity. In the growth temperature region between 473 and 673 K, the crystallinity degrades dramatically. XRD profiles indicate that the uniformity of crystallographic orientation is randomized above the growth temperature of 573 K. The degradation of crystallinity promotes the broadening of energy barrier distribution, together with the broadening of size distribution. Thus, the observed broadening of size distribution and the degradation of crystallinity could explain the change of dominant factor of ZFC magnetization.

ACKNOWLEDGMENTS

This work is supported by a Grant-in-Aid for General Scientific Research (S), Encouragement of Young Scientists (B), and Priority Assistance for the Formation of Worldwide Renowned Centers of Research—The Global COE Program (Project: Center of Excellence for Advanced Structural and Functional Materials Design) from the Ministry of Education, Culture, Sports, Science and Technology (MEXT), Japan.

*Corresponding author. shiratsuchi@mat.eng.osaka-u.ac.jp

[1] J. L. Dormann, D. Fiorani, and E. Tronc, Adv. Chem. Phys. **98**, 283 (1997).
[2] V. Skumryev, S. Stoyanov, Y. Zhang, G. Hajipanayis, D. Givord, and J. Nogués, Nature (London) **423**, 850 (2003).
[3] M. Bode, O. Pietzsch, A. Kubetzka, and R. Wiesendanger, Phys. Rev. Lett. **92**, 067201 (2004).
[4] L. H. F. Andrade, A. Laraoui, M. Vomir, D. Muller, J.-P. Stoquert, C. Estournès, E. Beaurepaire, and J.-Y. Bigot, Phys. Rev. Lett. **97**, 127401 (2006).
[5] H. F. Du, J. Appl. Phys. **99**, 104306 (2006).
[6] Y. Li, J. Magn. Magn. Mater. **303**, 243 (2006).
[7] Y. Shiratsuchi, M. Yamamoto, Y. Endo, D. Li, and S. D. Bader, J. Appl. Phys. **94**, 7675 (2003).
[8] Y. Shiratsuchi, Y. Endo, M. Yamamoto, and S. D. Bader, J. Appl. Phys. **95**, 6897 (2004).
[9] Y. Shiratsuchi, M. Yamamoto, and S. D. Bader, Prog. Surf. Sci. **82**, 121 (2007).
[10] L. Néel, Acad. Sci., Paris, C. R. **228**, 664 (1949).
[11] R. W. Chantrell, M. Eil-Hilo, and K. O'Grady, IEEE Trans. Magn. **27**, 3570 (1991).
[12] Y. Shiratsuchi, Y. Endo, and M. Yamamoto, Thin Solid Films **464-465**, 141 (2004).
[13] J. L. Dorman, D. Fiorani, and M. El Yamani, Phys. Lett. A **120**, 95 (1987).
[14] M. El-Hilo, K. O'Grady, and R. W. Chantrell, J. Magn. Magn. Mater. **114**, 307 (1992).
[15] S. Linderth, L. Balcells, A. Labarta, J. Tejada, P. V. Hendriksen, and S. A. Sethi, J. Magn. Magn. Mater. **124**, 269 (1993).
[16] W. Luo, S. R. Nagel, T. F. Rosenbaum, and R. E. Rosensweig, Phys. Rev. Lett. **67**, 2721 (1991).
[17] M. Hanson, C. Johansson, and S. Mørup, J. Phys.: Condens. Matter **7**, 9263 (1995).
[18] J. C. Denardin, A. L. Brandl, M. Knobel, P. Panissod, A. B. Pakhomov, H. Liu, and X. X. Zhang, Phys. Rev. B **65**, 064422 (2002).
[19] S. Shtrickman and E. P. Wohlfarth, Phys. Lett. **85A**, 467 (1981).
[20] O. Petracic, X. Chen, S. Bedanta, W. Kleemann, S. Sahoo, C. Cardoso, and P. P. Freitas, J. Magn. Magn. Mater. **300**, 192 (2006).
[21] H. Mamiya, I. Nakatani, and T. Furubayashi, Phys. Rev. Lett. **80**, 177 (1998).
[22] S. Sahoo, O. Petracic, Ch. Binek, W. Kleemann, J. B. Sousa, S. Cardoso, and P. P. Freitas, J. Phys.: Condens. Matter **14**, 6729 (2002).
[23] S. Sahoo, O. Petracic, W. Kleemann, P. Nordblad, S. Cardoso, and P. P. Freitas, Phys. Rev. B **67**, 214422 (2003).
[24] M. Sasaki, P. E. Jönsson, H. Takayama, and H. Mamiya, Phys. Rev. B **71**, 104405 (2005).